Geosci. Model Dev. Discuss., doi:10.5194/gmd-2016-259, 2016
Manuscript under review for journal Geosci. Model Dev.
Published: 24 October 2016

Geoscientific Model Development Discussions

A new module for trace gas emissions in ICON-ART 2.0: A sensitivity study focusing on acetone emissions and concentrations

Michael Weimer[1,2], Jennifer Schröter[2], Johannes Eckstein[2], Konrad Deetz[2], Marco Neumaier[2], Garlich Fischbeck[2], Daniel Rieger[2], Heike Vogel[2], Bernhard Vogel[2], Thomas Reddmann[2], Oliver Kirner[1], Roland Ruhnke[2], and Peter Braesicke[2]

[1]Steinbuch Centre for Computing, Karlsruhe Institute of Technology, 76344 Eggenstein-Leopoldshafen, Germany
[2]Institute of Meteorology and Climate Research, Karlsruhe Institute of Technology, 76344 Eggenstein-Leopoldshafen, Germany

Correspondence to: M. Weimer (michael.weimer@kit.edu)

Abstract. We present a new emissions module for the ICON (ICOsahedral Non-hydrostatic)-ART (Aerosols and Reactive Trace gases) modelling framework. The emissions module processes external flux data sets and increments the tracer volume mixing ratios in the boundary layer accordingly. In addition, the module for online calculations of biogenic emissions (MEGAN2.1) is implemented in ICON-ART and can replace the offline biogenic emission data sets.

The performance of the emissions module is illustrated with simulations of acetone, using a simplified chemical depletion mechanism based on a reaction with OH and photolysis only.

In our model setup, we calculate a tropospheric acetone lifetime of 33 days, which is in good agreement with the literature. We compare our results with airborne IAGOS-CARIBIC measurements in the upper troposphere and lowermost stratosphere (UTLS) in terms of phase and amplitude of the annual cycle. In all our ICON-ART simulations the general seasonal variability is well represented but questions remain concerning the magnitude of the acetone emissions and its atmospheric lifetime.

We conclude that the new emissions module performs well and allows the simulation of the annual cycles of emissions dominatedconcentrations even with a simple chemistry only.

1 Introduction

Many trace gases (called tracers hereafter) are emitted into the atmosphere by sources located at the Earth's surface. Especially for volatile organic compounds (VOCs), natural and anthropogenic emissions as well as secondary production from emitted precursor compounds are major atmospheric sources (e.g., Blake and Blake, 2002; Atkinson and Arey, 2003).

Two different approaches to account for emissions in atmospheric modelling have been developed in the past: The emission fluxes are either read from external data sets or calculated online with the possibility to account for the current state of the atmosphere in the model (e.g., Kerkweg et al., 2006; Keller et al., 2014).

In the previous version of the coupled modelling framework ICON-ART, only emissions of aerosols are considered (ICON: ICOsahedral Non-hydrostatic modelling framework, ART: Aerosols and Reactive Trace gases, Rieger et al., 2015; Zängl et al., 2015). A module accounting for trace gas emissions was not existing so far.

Geosci. Model Dev. Discuss., doi:10.5194/gmd-2016-259, 2016
Manuscript under review for journal Geosci. Model Dev.
Published: 24 October 2016

Geoscientific Model Development Discussions
Open Access
EGU

Here we present a new interface for including emissions from external data sources in ICON-ART which is independent of the temporal resolution of the underlying emission data. This interface reads emission mass fluxes from data sets, remapped to the unstructured ICON grid, and interpolates them to the ICON-ART simulation time. After conversion to volume mixing ratio (VMR) the emission is added to the tracer VMR in ICON-ART in the lowest model layers. This number is specified by the user.

In addition, the Model of Emissions of Gases and Aerosols from Nature (MEGAN2.1, Guenther et al., 2012) as implemented in ICON-ART is presented. This model calculates biogenic emissions of VOCs online, i.e. dependent on the current state of the atmosphere.

We also describe a new simplified mechanism for depletion of trace gases due to reaction with OH, the main tropospheric sink for most VOCs (Blake and Blake, 2002). This mechanism allows the space and time dependent calculation of the tracers' loss rate. Thus, these new developments now allow the investigation of VOCs with ICON-ART.

Several VOCs act as precursors of OH and HO_2 ($= HO_x$) radicals particularly in the dryer upper troposphere and lowermost stratosphere (UTLS) (Folkins and Chatfield, 2000). HO_x can deplete ozone so that VOCs have climatic impact in the UTLS region (e.g., Neumaier et al., 2014). In this study, we will focus on the influence of acetone which is together with methanol one the most abundant VOC in the UTLS region. Mixing ratios of $300 - -2000\,\mathrm{pptv} (1\,\mathrm{pptv} = 10^{-12}\mathrm{mol\,mol^{-1}})$ have been observed in the Northern Hemisphere midlatitudes (Singh et al., 1995; Jaeglé et al., 1998; Heikes et al., 2002; Sprung and Zahn, 2010; Elias et al., 2011; Neumaier et al., 2014).

This study is organised as follows: In Sect. 2 the model ICON with its ART extension is described followed by the description of the new emission interface in ICON-ART in Sect. 3. Then, the simplified mechanism for VOC depletion is introduced (Sect. 4). After a description of the IAGOS-CARIBIC project and the simulations for this study in Sections 5 and 6, the results are presented in Sect. 7 followed by conclusions and an outlook (Sect. 8).

2 The ICON model with its ART extension

In this section, we briefly describe the ICON model (Sect. 2.1) and its ART extension (Sect. 2.2). More detailed descriptions can be found in Zängl et al. (2015) and Rieger et al. (2015), respectively.

2.1 The ICON model

ICON is a non-hydrostatic atmospheric model which is currently under development with the aim of providing a global model for both weather and climate (Wan et al., 2013; Zängl et al., 2015).

Horizontal discretisation is performed on an icosahedral-triangular C grid. In contrast to to the regular latitude-longitude grid, this is an unstructured grid where the grid points are saved as one-dimensional arrays.

In this study, we use the same resolution notation as introduced by Zängl et al. (2015): RnBk with n and k as indicators for root division and bisections, respectively. Usual resolutions and the corresponding global number of grid cells are shown in Table 1.

Geosci. Model Dev. Discuss., doi:10.5194/gmd-2016-259, 2016
Manuscript under review for journal Geosci. Model Dev.
Published: 24 October 2016

Geoscientific Model Development Discussions
Open Access
EGU

Table 1. Examples of ICON resolutions with characteristic length and total number of cells (from Zängl et al., 2015). Characteristic length and number of cells are calculated according to $\overline{\Delta x} = \sqrt{\pi/5}\,R/(n\,2^k)$ and $n_c = 20\,n^2\,4^k$ (R = Earth's radius and n and k as ICON resolution indicators). The grid number denotes the official ICON grid number for the grid configuration used in this study, rotated by 36 degrees around z-axis.

resolution	$\overline{\Delta x}$ (in km)	number of cells	grid number
R2B04	157.8	20 480	0012
R2B05	78.9	81 920	0014
R2B06	39.5	327 680	0016
R2B07	19.7	1 310 720	0018
R3B07[a]	13.9	2 949 120	0022

[a] global operational resolution at DWD

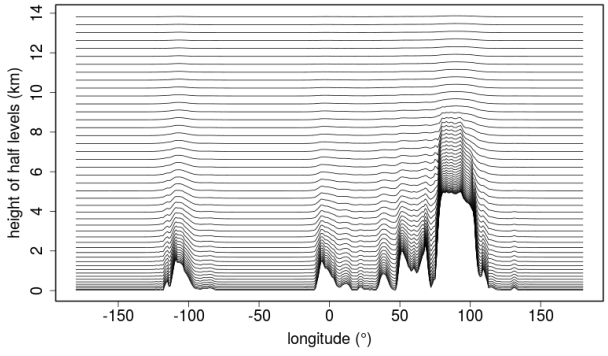

Figure 1. Height of the lowest 46 ICON model layers at 33° N in the configuration with 90 total model layers.

In the vertical, smooth-level coordinates as described by Leuenberger et al. (2010) are used (see Fig. 1).

In ICON tracers are transported by solving the continuity equation of mass for each tracer discretised with a time-split method: Finite volume method is used in the vertical whereas a simplified flux-form semi-Lagrangian method is used for horizontal transport (Miura, 2007; Lauritzen et al., 2011; Rieger et al., 2015).

Current tracers in ICON are water vapour and hydrometeors depending on the chosen microphysics scheme. In this study, the microphysics scheme is based on that used in COSMO (COnsortium for SMall-scale MOdelling, Doms and Schättler, 2004) and described in the technical documentation as part of the ICON source code (Seifert, 2010).

The tropopause height will play an important role in this study. In our simulations, it is calculated by ICON routines according to the thermal definition of World Meteorological Organization (WMO) (1957).

Geosci. Model Dev. Discuss., doi:10.5194/gmd-2016-259, 2016
Manuscript under review for journal Geosci. Model Dev.
Published: 24 October 2016

Geoscientific Model Development Discussions
Open Access
EGU

2.2 The ART module

The ART module for ICON is currently under development with the following aims (Rieger et al., 2015):

- Treatment of aerosols and gas-phase species in global modelling
- Gas-phase and heterogeneous chemistry
- Investigation of the feedbacks between aerosols, trace gases and the state of the atmosphere

Tracers in ICON-ART are transported and diffused in the same way as the internal ICON tracers like water vapour. The ICON-ART tracers used in this study include methane (CH_4), carbon monoxide (CO), propane (C_3H_8) and acetone ($CH_3C(O)CH_3$).

Chemical reactions are calculated according to the following equation:

$$\frac{\partial \overline{\rho}\hat{\psi}_i}{\partial t} = -A_i + P_i - L_i + E_i \tag{1}$$

where ρ, ψ_i, A_i and P_i are air density, partial density fraction, advection and chemical production of the tracer i, respectively. The hat over ψ denotes the barycentric average.

E_i and L_i are emission and loss rate of tracer i, respectively. In version 1.0 of ICON-ART (Rieger et al., 2015), no general algorithm for including E_i was included and the lifetime and therefore L_i was assumed to be globally constant. In version 2.0 used here, we added an interface for emissions (see Sect. 3) and a simplified OH chemistry for calculation of the loss rate (see Sect. 4).

Additionally, we implemented the predictor-corrector method according to Seinfeld and Pandis (2012) to solve Eq. (1) for tracer depletion via reaction with OH. This method is more accurate than that described by Rieger et al. (2015). A detailed description of the predictor-corrector method can be found in Appendix A.

3 The new emission interface in ICON-ART

We have included modules for offline and online calculation of emissions in ICON-ART. Both approaches are described in this section. In Section 3.1, we demonstrate our method to read and treat offline emissions whereas the description of the MEGAN2.1 model for online calculation of biogenic emissions in the configuration for ICON-ART follows in Sect. 3.2.

3.1 Offline emissions

Offline emissions in ICON-ART are calculated with a new module for including emissions from external data sources which is described in the following. The process can be separated into four steps (see Fig. 2): pre-processing, initialisation, reading and finalisation.

Pre-processing (Sect. 3.1.1) is required before the model run and includes horizontal interpolation of the input data to the ICON grid as well as preparation of meta information of the data set which is committed to the interface during initialisation.

Geosci. Model Dev. Discuss., doi:10.5194/gmd-2016-259, 2016
Manuscript under review for journal Geosci. Model Dev.
Published: 24 October 2016

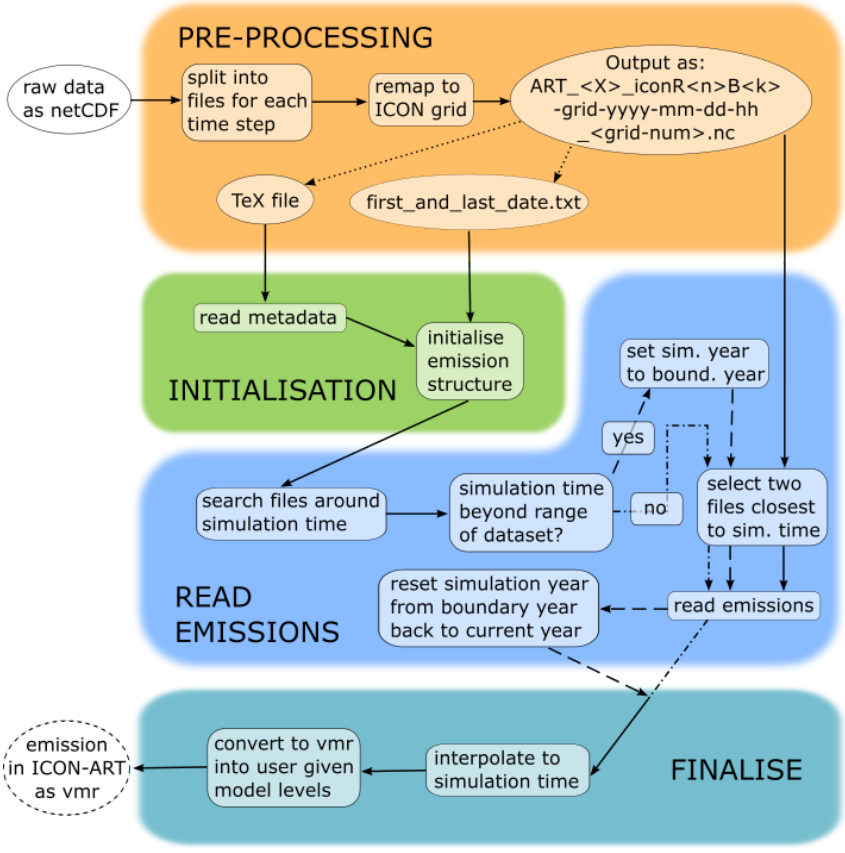

Figure 2. Flow chart of the process from the external netCDF emission data with regular grid and emission data as mass flux density to the emission as VMR in ICON-ART. The process can be separated into four steps: pre-processing, initialisation, read emissions and finalise the interface. Pre-processing before the run of ICON-ART is necessary whereas the other processes are included in ICON-ART. Ellipses depict files while rectangles stand for processes. The different arrow lines illustrate either the interaction with the remapped netCDF data set which has to be performed by the user in the pre-processing step (dotted), the "no" path (dotted and dashed) or the "yes" path (dashed).

Geosci. Model Dev. Discuss., doi:10.5194/gmd-2016-259, 2016
Manuscript under review for journal Geosci. Model Dev.
Published: 24 October 2016

Table 2. Notation of the abbreviations used for different types of emissions denoted as X in the name structure of the files together with the corresponding integer value used in ICON-ART.

type	abbreviation	integer value
anthropogenic	ANT	10
biogenic	BIO	11
biomass burning	BBE	12
biogenic online	ONL	13

The other steps are preformed automatically during operation of the model. In the step for reading emission (Sect. 3.1.2), the closest emission dates are searched and the emissions are interpolated to the current simulation time of ICON-ART. Finally, the temporally interpolated emission mass flux density is converted to VMR and added to the tracer VMR into user given number of model layers (Sect. 3.1.3).

In addition, we briefly describe the offline emission inventories used for this study (Sect. 3.1.4) and demonstrate the performance of the module (see Sect. 3.1.5).

3.1.1 Pre-processing of the input data and initialisation of the module

Due to the unstructured icosahedral grid of ICON (see Sect. 2.1), the usually structured latitude-longitude grid of emission data sets has to be interpolated to the ICON grid. This is managed by tools provided by German Weather Service (DWD) called the DWD ICON tools (Prill, 2016). In general, emissions are spatially highly variable. Therefore, the nearest neighbour interpolation method is applied which reasonably captures the spatial variability of the emissions and which also conserves the total emission flux reasonably.

With the current version of ICON-ART, it is only possible to read files consisting of one time step. That is why the emission data have to be separated into single files for each time step.

The files to be read by the emission interface have to follow the general ICON-ART name convention:

ART_<X>_iconR<n>B<k>-grid-
yyyy-mm-dd-hh_<grid-num>.nc

where <X> characterises the three character abbreviation of the emission type (see Table 2), and <n> and <k> are the ICON resolution indicators in the same format as in Table 1. Additionally, the date of the emission and the grid number (see Table 1) are part of the name structure. The maximum temporal resolution of the data set is hourly and every file can include emission data of more than one species.

Emission mass flux densities in units of $\mathrm{kg\,m^{-2}\,s^{-1}}$ are required in the raw data as the values are automatically converted to VMR after the reading process, see Sect. 3.1.3.

Geosci. Model Dev. Discuss., doi:10.5194/gmd-2016-259, 2016
Manuscript under review for journal Geosci. Model Dev.
Published: 24 October 2016

Geoscientific Model Development Discussions

```
\begin{table}[h] \caption{Chemical Tracers and their emission folders. Type of emission: 10
    \begin{tabular}{l r c c l}\\
    \hline
    Name     & number of types / type of emission & standard value (in kg m$^{-2}$ s$^{-1}$)
    \hline
TRCO_chemtr       & 0  &  0.00E+01  &  &  & \\
TRCH3COCH3_chemtr & 3  &  0.00E+01  &  &  & \\
          & 10 & 2 & 1 & acetone    & /path/to/anthropogenic/emission/data \\
          & 13 &   & 1 &            & /path/to/pft/data \\
          & 12 & 2 & 1 & acetone    & /path/to/biomass/burning//emission/data \\
```

Figure 3. Sample extract of a TeX table committing emission metadata to the module. Details see text.

The controlling TeX table and "first_and_last_date.txt"

Some meta information have to be committed to the module, e.g. about the data set's location on the disk and the variable name in the remapped netCDF file for each emission data set and each tracer in ICON-ART. These metadata are controlled by a TeX table (see Fig. 3).

In the simplest form, each tracer in the TeX table is represented by one line (see tracer CO in Fig. 3). This line contains the tracer name (column 1), the number of emissions to be considered (column 2) and the standard value as mass flux density (column 3). This is taken into account only the number of emissions is zero and is then used globally. Then one line per emission follows with empty first column, each giving the following:

- column 2: emission type as integer (see Table 2)
- column 3: number of dimensions of the emission data in the file without the time dimension: 2 or 3, for two or three dimensional data
- column 4: number of lowest model layers into which emission shall be included
- column 5: variable name in the netCDF files
- column 6: full path to the netCDF files

In the example of Fig. 3, no emission data sets are considered for CO. Since the standard emission value is set to zero as well, no emissions are computed for CO at all. For acetone, offline and online emissions have to be considered. The anthropogenic (type is set to 10, see Table 2) and biomass burning data set (type 12) are both two-dimensional emissions to be included in one (i.e. the lowest) model layer and with the variable name "acetone" in the netCDF files. Biogenic emissions in this example are calculated online (type 13). They are also added to the lowest model layer. The path for online emissions refers to the data set of plant functional types (see Sect. 3.2).

If the simulation time exceeds the range of the data set the boundary year is repeated as long as necessary (see Fig. 2 in the "read emission" step). That is why the boundary dates of the data set also have to be committed to the module. For this, the ASCII file "first_and_last_date.txt" placed in the same folder as the data set is used containing the first and the last date of the data set in the ICON date format in separate lines as shown in Fig. 4.

Geosci. Model Dev. Discuss., doi:10.5194/gmd-2016-259, 2016
Manuscript under review for journal Geosci. Model Dev.
Published: 24 October 2016

Geoscientific Model Development Discussions
Open Access
EGU

```
1980-01-01T00:00:00Z
2010-12-01T00:00:00Z
```

Figure 4. Content of "first_and_last_date.txt". It commits the boundary dates of the data set to the module with first date of data set in the first line and last date in the second one. Here, an example is given for the inventory MEGAN-MACC (see Sect. 3.1.4 for further information).

3.1.2 Reading emissions

The first task of the module during operation is to find the two emission dates closest to the simulation time. For this, one hour is successively added to or subtracted from the simulation time until a file at that date is found. The next file is searched only if the simulation time exceeds the date of the later emission file.

Apart from limits of the temporal resolution, no further assumptions of the data set's temporal resolution have to be made. Missing files or variable temporal resolution of the data are possible and taken care of by the model. As mentioned in Sect. 3.1.1, the lower limit of the temporal resolution is hourly. ICON-ART aborts when no file is found before or after 10^5 hours (about 11 years) with a corresponding error message.

3.1.3 Time interpolation of the emissions and conversion to VMR

The maximum temporal resolution of the data is hourly (see Sect. 3.1.1) but the model time steps in ICON-ART are in the order of minutes for resolution R2B04 or below for higher resolutions. Therefore, the emission data is linearly interpolated to the simulation time.

After interpolation the emission is converted to VMR ($C_{\mathrm{emi},i}$) according to:

$$C_{\mathrm{emi},i} = \frac{n_i}{n_{\mathrm{air}}} = \frac{E_i \, \Delta t \, R^*}{M_i} \cdot \left(\sum_{l=k_{\mathrm{lev}}}^{k_{\mathrm{lev}}-k_{\mathrm{emi}}-1} \frac{p_l \, h_l}{T_l} \right)^{-1} \tag{2}$$

In this equation for one model grid box, the number of moles of the emission n_i of tracer i is divided by the number of moles of the air n_{air}. The moles of emission n_i are calculated as emission mass flux density E_i multiplied by the model time step Δt and the base area of the grid box (cancels out during division with n_{air}) and divided by the molar mass of the tracer M_i. The moles of air n_{air} are calculated via air density multiplied by the volume of the grid box (base area A times height h_l) and divided by the molar mass of the air M_{air} which cancels out when replacing the air density with the ideal gas law:

$$n_{\mathrm{air},l} = \frac{\rho_{\mathrm{air},l} \, A \, h_l}{M_{\mathrm{air}}} = \frac{p_l \, A \, h_l}{M_{\mathrm{air}} \, R_{\mathrm{air}} \, T_l} = \frac{A}{R^*} \frac{p_l \, h_l}{T_l} \tag{3}$$

Accordingly, p_l, T_l and R^* in Eqs. (2) and (3) stand for pressure and temperature of the grid box and the universal gas constant, respectively. The resulting emission VMR of Eq. (2) is added to the tracer VMR in the user specified number of lowest model layers k_{emi}. In Equation (2), k_{lev} represents the total number of model layers (90 in our configuration of ICON-ART).

Geosci. Model Dev. Discuss., doi:10.5194/gmd-2016-259, 2016
Manuscript under review for journal Geosci. Model Dev.
Published: 24 October 2016

Geoscientific Model Development Discussions

Table 3. Technical details of the emission inventories from ECCAD for tracers in ICON-ART. For abbreviations of the emission types, see Table 2.

inventory	type	time range	resolution		tracers			
			space	time	CH_4	CO	C_3H_8	$CH_3C(O)CH_3$
MACCity[a]	ANT	1960-2020	0.5°	month	-	✓	✓	✓
EDGARv4.2[b]	ANT	1970-2008	0.5°	year	✓	-	-	-
MEGAN-MACC[c]	BIO	1980-2010	0.5°	month	✓	✓	✓	✓
GFED3[d]	BBE	1997-2010	0.5°	month	✓	✓	✓	✓

[a] Lamarque et al. (2010), Diehl et al. (2012), Granier et al. (2011) and van der Werf et al. (2006),
[b] Janssens-Maenhout et al. (2011, 2013), [c] Sindelarova et al. (2014), [d] van der Werf et al. (2010)

This method conserves mass of the emission since the calculated moles of the emission do not change if k_{emi} is increased. The emission is just distributed in a larger column.

3.1.4 Emission inventories

The emission data for the tracers used in this study can be downloaded from the database of Emissions of atmospheric Compounds & Compilation of Ancillary Data (ECCAD, http://eccad.sedoo.fr). The inventories used for this study are MACCity, EDGARv4.2, MEGAN-MACC and GFED3 and will be described briefly in the following paragraphs. The emission inventories are chosen according to length and temporal resolution of the data. A summary of the technical details of each used emission inventory is shown in Table 3. This table also shows which inventory is used for which tracer.

The inventory MACCity includes monthly anthropogenic and biomass burning emissions (Granier et al., 2011). The anthropogenic emission data are taken from the historical monthly data set of Atmospheric Chemistry and Climate Model Intercomparison Project (ACCMIP), described by Lamarque et al. (2010), and the Representative Concentration Pathways 8.5 (RCP8.5) emission scenario.

In the anthropogenic inventory Emissions Database for Global Atmospheric Research version 4.2 (EDGARv4.2, Janssens-Maenhout et al., 2011, 2013) emissions are calculated with a country-sector method based on emission factors and more than 50 categories of anthropogenic emission sources (for more information see http://edgar.jrc.ec.europa.eu/methodology.php).

For the inventory MEGAN-MACC (Sindelarova et al., 2014), monthly mean biogenic emissions are calculated with MEGAN2.1 and the same 15 plant functional types as in our configuration (see Sect. 3.2). Meteorological fields are taken from the Goddard Earth Observing System (GEOS) and assimilated to model space. The leaf area index is derived from MODIS retrievals.

Biomass burning emissions in the inventory called Global Fire Emissions Database version 3 (GFED3, van der Werf et al., 2010) are calculated with a modified version of the Carnegie Ames Stanford Approach model (CASA, Potter et al., 1993; Field et al., 1995; Randerson et al., 1996). Several fire emission types are derived from satellite data and combined for calculating

Geosci. Model Dev. Discuss., doi:10.5194/gmd-2016-259, 2016
Manuscript under review for journal Geosci. Model Dev.
Published: 24 October 2016

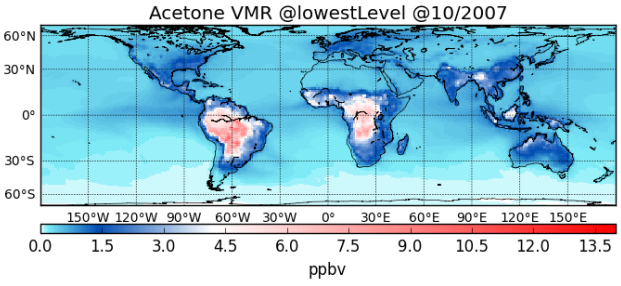

Figure 5. Monthly mean acetone volume mixing ratio in the lowest model layer (layer 90, height of about 20 m above surface) for October 2007, more than 3 years after initialisation of the constL(off) simulation (see Sect. 6).

the carbon emission flux on a monthly basis in each grid cell. The emission flux for the substances is calculated using emission factors depending on the type of fire.

In the used inventories, acetone emissions are dominated by biogenic emissions. Anthropogenic and biomass burning emissions amount for 3 % and 5 % of the total global acetone emission, respectively. These values are consistent with the values published by Jacob et al. (2002) and Fischer et al. (2012).

3.1.5 Performance of the offline module

We demonstrate the performance of the module by including offline emissions for acetone as described in Table 3. Figure 5 shows the monthly mean acetone VMR in the lowest model layer for October 2007 for the case of a constant lifetime of 28 days. As biogenic emissions dominate the acetone emissions, the maximum values in the acetone VMR occur over Central Africa and South America where the biogenic emissions of the inventory MEGAN-MACC also are maximised (not shown).

3.2 Online biogenic emissions: MEGAN2.1

To account for the influence of temperature, vegetation and photosynthetically active radiation (PAR) on the emission of acetone, the Model of Emissions of Gases and Aerosols from Nature version 2.1 (MEGAN2.1, MEGAN-Online hereafter) (Guenther et al., 2012) was implemented into ICON-ART. In contrast to the external acetone data sets (here MEGAN-MACC) which are given as monthly mean values, the online calculation of acetone emissions within Guenther et al. (2012) allows to account for the current conditions in meteorology (especially the diurnal cycle) and vegetation. The parametrisation of biogenic emissions including acetone is described in detail in Guenther et al. (2012), therefore we present here only the main concept of the parametrisation, the changes we have made and the input provided to MEGAN-Online.

Geosci. Model Dev. Discuss., doi:10.5194/gmd-2016-259, 2016
Manuscript under review for journal Geosci. Model Dev.
Published: 24 October 2016

Geoscientific Model Development Discussions
Open Access
EGU

MEGAN-Online estimates the biogenic emission mass flux density F in $\mu g\,m^{-2}\,h^{-1}$ of the compound class c via the following equation:

$$F_c = \gamma_c \sum_j \epsilon_{c,j}\,\chi_j, \tag{4}$$

where $\epsilon_{c,j}$ is the emission factor depending on the vegetation type j with the fractional grid box coverage χ_j. The emission activity factor γ_c accounts for environmental and phenological conditions which affect the emissions.

MEGAN-Online includes 19 compound classes but the study on hand will focus on acetone ($c = 13$). Guenther et al. (2012) consider the emission affecting processes due to light, temperature, leaf age, soil moisture, leaf area index and CO_2 inhibition. The implementation in ICON-ART only accounts for the emission responses from light, temperature, leaf area index (LAI) and leaf age.

The light is provided by ICON-ART as photosynthetically active radiation (PAR) and temperature in the lowest model layer is a standard meteorological variable of ICON-ART. The leaf area index is based on external parameters read during initialisation of ICON-ART. The leaf age considers the fraction of new (FNEW), growing (FGRO), mature (FMAT) and senescing (FSEN) leaves. Due to missing information about the global distribution of these four leaf types, we assumed a uniform distribution. In addition to the standard LAI we have included the parametrisation of Dai et al. (2004) to derive LAI_{sun}, the LAI that is lit by sun, since only this leaf fraction can emit biogenic VOCs:

$$LAI_{\mathrm{sun}} = \frac{1}{k_b}\left(1 - \exp\left(-k_b\,LAI\right)\right) \tag{5}$$

with $k_b = G(\mu,\theta)/\mu$. μ is the cosine of the solar zenith angle and $G(\mu,\theta)$ is a function depending on μ and an empirical parameter θ related to the leaf angle distribution. In the following we assume a random distribution of leaf angles which leads to $G(\mu,\theta) = 0.5$. The solar zenith angle is provided by ICON-ART. LAI_{sun} was added to MEGAN-Online because Dai et al. (2004) have shown that the net photosynthetic rate of sunlit leaves is relatively high due to light saturation whereas a drastic reduction of the photosynthetic rate is visible in the low light layers of shaded leaves. With LAI_{sun} we therefore want to avoid an overestimation of the biogenic emissions especially in areas with high LAI which is linked to a high layering of the leaves (e.g. tropical rain forest).

To consider the vegetation type we use the external plant functional type (PFT) data set provided by the Community Climate System Model (CCSM) (https://svn-ccsm-inputdata.cgd.ucar.edu/trunk/inputdata/lnd/clm2/rawdata/) for 2005 with a grid mesh size of $0.05°$. This PFT data set follows the vegetation class definition of Guenther et al. (2012). The main idea of using PFTs instead of classical vegetation types is to cluster vegetation types with similar biogenic emission characteristics into the same groups for which then the emission factors $\epsilon_{c,j}$ can be defined.

In addition, MEGAN-Online needs averaged information about PAR and leaf temperature. Highest acetone emissions are observable in tropical regions and therefore we have estimated these values according to this climate zone. The mean Photosynthetic Photon Flux Density (PPFD) over 24 hours (PPFD24) and 240 hours (PPFD240) is estimated to $400\,\mu mol\,m^{-2}\,s^{-1}$

Geosci. Model Dev. Discuss., doi:10.5194/gmd-2016-259, 2016
Manuscript under review for journal Geosci. Model Dev.
Published: 24 October 2016

Geoscientific Model Development Discussions

Table 4. Parameters for MEGAN-Online used for this study. Time dependent parameters are written in italic letters.

Variable/Parameter	Units	Selection in ICON-ART	Meaning
T	K	Standard ICON-ART output	Temperature at lowest model layer
PAR	$\mathrm{W\,m^{-2}}$	Standard ICON-ART output	Photosynthetically active radiation
SZA	degrees	Standard ICON-ART output	Sun zenith angle
LAI	$\mathrm{m^2\,m^{-2}}$	External data from EXTPAR	Leaf area index
PFT	1	External data from CCSM	Plant functional type
PPFD	$\mu\mathrm{mol\,m^{-2}\,s^{-1}}$	Derived from PAR	Photosynthetic Photon Flux Density
PPFDS	$\mu\mathrm{mol\,m^{-2}\,s^{-1}}$	125	Standard conditions for PPFD averaged over last 24 h
PPFD24	$\mu\mathrm{mol\,m^{-2}\,s^{-1}}$	400	PPFD averaged over last 24 h
PPFD240	$\mu\mathrm{mol\,m^{-2}\,s^{-1}}$	400	PPFD averaged over last 240 h
T24	K	297	Average leaf temperature of the past 24 h
T240	K	297	Average leaf temperature of the past 240 h
FNEW	1	0.25	Fraction of new foliage
FGRO	1	0.25	Fraction of growing foliage
FMAT	1	0.25	Fraction of mature foliage
FSEN	1	0.25	Fraction of senescing foliage
G(μ,θ)	1	0.5	function for LAI_{sun} depending on SZA and leaf angle distribution

from a simulation study. The mean leaf temperature over 24 hours (T24) and 240 hours (T240) is estimated to 297 K also based on a simulation study. The above mentioned values are not available as regular variables in ICON-ART and therefore have to be estimated (spatiotemporally constant). This could be a further source of uncertainty among the overestimation of the LAI.

For standard conditions the Photosynthetic Photon Flux Density (PPFDS) is between $50\,\mu\mathrm{mol\,m^{-2}\,s^{-1}}$ for shaded leaves and $200\,\mu\mathrm{mol\,m^{-2}\,s^{-1}}$ for sun leaves (Guenther et al., 2012). For this study we use the average of $125\,\mu\mathrm{mol\,m^{-2}\,s^{-1}}$. Table 4 summarises the input of MEGAN-Online and the parameter selection as used for this study.

In the following we compare the results from three emission scenarios: MEGAN-MACC, MEGAN-Online LAI and MEGAN-Online LAI_{sun}. MEGAN-MACC uses the emissions from the external data set. MEGAN-Online uses the online calculated emissions by using LAI (MEGAN-Online LAI) and the LAI that is lit by sun (MEGAN-Online LAI_{sun}).

Figure 6 shows the results of the three emission scenarios. The biogenic emission inventory MEGAN-MACC consists of monthly mean values of the MEGAN2.1 model (see Sect. 3.1.4). Therefore, the diurnal cycle is neglected in the inventory. The time series in Fig. 6 are spatially averaged over South America where the global maximum of biogenic emissions occurs, see Fig. 5. The inventory MEGAN-MACC, represented by the black dashed line in Fig. 6, is linearly interpolated between October

Geosci. Model Dev. Discuss., doi:10.5194/gmd-2016-259, 2016
Manuscript under review for journal Geosci. Model Dev.
Published: 24 October 2016

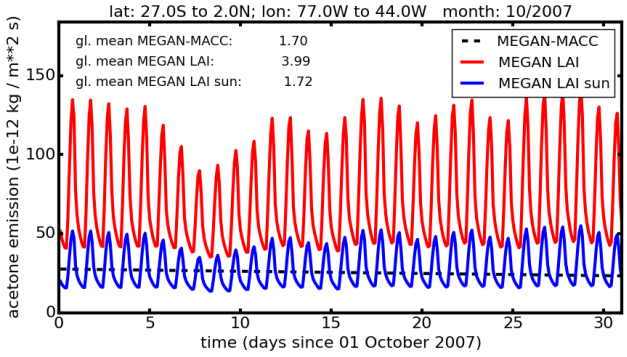

Figure 6. Acetone emission comparison of MEGAN-MACC (black dashed), MEGAN-Online LAI (red) and MEGAN-Online LAI_{sun} (blue) averaged over South America (77 to 44° W and 27° S to 2° N) in October 2007. The mean values represent global means in $10^{-12}\,\mathrm{kg\,m^{-2}\,s^{-1}}$ including the sea where the emissions are zero. The written mean of MEGAN-MACC is the global mean of the first time step in the time series as the MEGAN-MACC emissions already are monthly means.

and November. However, as acetone is emitted as by-product of photosynthesis (Jacob et al., 2002), the diurnal cycle in the emission should be considered.

With online emissions, it is now possible to capture the diurnal cycle in the emissions of acetone. The acetone online emissions are non-zero during the night which is consistent with the literature (e.g., Shao and Wildt, 2002).

The emissions of the MEGAN-Online LAI scenario are more than twice higher than that of MEGAN-MACC. In contrast to this, the emissions due to LAI_{sun} of Eq. (5) have the same global mean as MEGAN-MACC (considering the uncertainties in MEGAN-MACC). This means that this parametrisation can be used for investigation of the effect of the diurnal cycle on the emissions and the acetone VMR in the atmosphere.

4 Parametrisation of tracer depletion with simplified OH chemistry

The main atmospheric sink for VOCs is the reaction with OH. Here, we illustrate the new OH depletion mechanism as implemented in ICON-ART. This parametrisation calculates the tracers' loss rate dependent on space and time and can replace the globally constant lifetime as mentioned in Rieger et al. (2015). As an example, we illustrate the mechanism with acetone as one member of the VOCs.

4.1 Troposphere and UTLS region

As the tracer depletion mechanism by reaction with OH, described below, includes photolysis of ozone we first explain how photolysis rates are treated in ICON-ART.

Photolysis rates in ICON-ART are calculated by the photolysis module which provides precise online calculation of 72 photolytic reactions including an interface between ICON, ICON-ART and the Cloud-J package (Prather, 2015). The impact

Geosci. Model Dev. Discuss., doi:10.5194/gmd-2016-259, 2016
Manuscript under review for journal Geosci. Model Dev.
Published: 24 October 2016

of clouds and aerosols can be taken into account via different approaches implemented in the module and within Cloud-J. Cloud properties like cloud water path and effective radius of cloud droplets are calculated using ICON micro-physical properties. Cross sections and quantum yields are given in a tabulated form, generated by an interpolation algorithm which uses Sander et al. (2011). The overhead ozone column, that is used, is based on the climatology of Global and regional Earth-system (Atmosphere) Monitoring using Satellite and in-situ data (GEMS, Hollingsworth et al., 2008).

The photolysis module covers roughly the wavelength region from $170\,\mathrm{nm}$ up to $850\,\mathrm{nm}$, binned into 18 wavelength bins. Thus, it is possible to accurately calculate photolysis rates from the troposphere up to the stratosphere. For the simulations within this study the average cloud mode of Cloud-J is used.

The tropospheric OH concentration is calculated according to a simplified model, shown e.g. by Jacob (1999), see Reactions (R1) to (R8). In this model, ozone is photolysed producing an oxygen atom in excited state, $\mathrm{O(^1D)}$. $\mathrm{O(^1D)}$ either is quenched by collision with nitrogen ($\mathrm{N_2}$) or oxygen ($\mathrm{O_2}$) or reacts with $\mathrm{H_2O}$, leading to two OH radicals:

$$\mathrm{O_3 + h\nu \xrightarrow{J_{O_3}} O(^1D) + O_2} \tag{R1}$$
$$\mathrm{N_2 + O(^1D) \xrightarrow{k_{N_2}} O(^3P) + N_2} \tag{R2}$$
$$\mathrm{O_2 + O(^1D) \xrightarrow{k_{O_2}} O(^3P) + O_2} \tag{R3}$$
$$\mathrm{H_2O + O(^1D) \xrightarrow{k_{H_2O}} 2OH} \tag{R4}$$

OH is depleted by reaction with either $\mathrm{CH_4}$ or CO, the main sinks for OH (Jacob, 1999):

$$\mathrm{OH + CH_4 \xrightarrow{k_{CH_4}} H_2O + CH_3} \tag{R5}$$
$$\mathrm{\longrightarrow \cdots \longrightarrow CO + HO_2} \tag{R6}$$
$$\mathrm{OH + CO \xrightarrow{M,k_{CO,1}} H + CO_2} \tag{R7}$$
$$\mathrm{OH + CO \xrightarrow{M,k_{CO,2}} HOCO} \tag{R8}$$

Reaction rates and photolysis rates in this study are denoted as k and J, respectively. In the following, squared brackets stand for number concentration of the species. According to the reaction system above, the steady state OH concentration is calculated by the following equation (cf. Jacob, 1999; Dunlea and Ravishankara, 2004; Elshorbany et al., 2016):

$$[\mathrm{OH}] = \frac{2\,[\mathrm{O(^1D)}]\,k_{\mathrm{H_2O}}\,[\mathrm{H_2O}]}{k_{\mathrm{CH_4}}\,[\mathrm{CH_4}] + (k_{\mathrm{CO},1} + k_{\mathrm{CO},2})\,[\mathrm{CO}]} \tag{6}$$

where $[\mathrm{O(^1D)}]$ is calculated by assuming a steady state with Reactions (R1) to (R4) resulting in the following formula:

$$[\mathrm{O(^1D)}] = \frac{J_{\mathrm{O_3}}\,[\mathrm{O_3}]}{k_{\mathrm{O_2}}\,[\mathrm{O_2}] + k_{\mathrm{N_2}}\,[\mathrm{N_2}] + k_{\mathrm{H_2O}}\,[\mathrm{H_2O}]} \tag{7}$$

Geosci. Model Dev. Discuss., doi:10.5194/gmd-2016-259, 2016
Manuscript under review for journal Geosci. Model Dev.
Published: 24 October 2016

Geoscientific Model Development Discussions
Open Access
EGU

In Equations (6) and (7), the O_3 photolysis rate J_{O_3} is calculated by the online photolysis module in ICON-ART (see above in this section). Ozone is provided by the GEMS climatology (Hollingsworth et al., 2008). $[H_2O]$ is calculated as part of the ICON micro-physics (see Sect. 2.1). O_2 and N_2 VMRs are set to $20.946\,\%$ and $78.084\,\%$, respectively (Brasseur and Solomon, 1995), and converted to number concentrations. The reaction rates in Eqs. (6) and (7) are taken from Sander et al. (2011).

With Equation (6), the loss rates of CO, CH_4 and C_3H_8 are calculated as follows:

$$L_i = k_i\,[\mathrm{OH}], \quad i \in \{\mathrm{CO}, \mathrm{CH_4}, \mathrm{C_3H_8}\} \tag{8}$$

A chemical production of CO due to Reaction (R5) is considered in this study (see Reaction (R6)) as this reaction is the main source for atmospheric CO (Jacob, 1999; Boucher et al., 2001; Seinfeld and Pandis, 2012):

$$P_{\mathrm{CO}} = k_{\mathrm{CH4}}\,[\mathrm{OH}]\,[\mathrm{CH_4}] \tag{9}$$

As an example, we will focus on acetone in the following. Acetone is depleted either by reaction with OH or by photolysis where two channels have to be considered:

$$\mathrm{CH_3C(O)CH_3 + OH} \xrightarrow{\mathrm{k_{acetone}}} \mathrm{Products} \tag{R9}$$

$$\mathrm{CH_3C(O)CH_3 + h\nu} \xrightarrow{\mathrm{J_{acetone,1}}} \mathrm{CH_3CO + CH_3} \tag{R10}$$

$$\mathrm{CH_3C(O)CH_3 + h\nu} \xrightarrow{\mathrm{J_{acetone,2}}} \mathrm{2CH_3 + CO} \tag{R11}$$

Reaction (R9) has different channels and is abbreviated here. For the reaction rate k_{acetone}, we use the recommended formula of Sander et al. (2011).

Following Reactions (R9) to (R11), the loss rate of acetone is determined by:

$$L_{\mathrm{acetone}} = k_{\mathrm{acetone}}\,[\mathrm{OH}] + J_{\mathrm{acetone},1} + J_{\mathrm{acetone},2} \tag{10}$$

We use the mass-weighted mean shown by SPARC (2013) to calculate the lifetime of acetone:

$$\tau_{\mathrm{acetone}} = \frac{\int [\mathrm{CH_3C(O)CH_3}]\,\mathrm{d}V}{\int L_{\mathrm{acetone}} \cdot [\mathrm{CH_3C(O)CH_3}]\,\mathrm{d}V} \tag{11}$$

Additionally, the chemical production of acetone due to reaction of propane (C_3H_8) with OH is considered:

$$P_{\mathrm{acetone}} = 0.736\,[\mathrm{C_3H_8}]\,[\mathrm{OH}]\,k_{\mathrm{C_3H_8}} \tag{12}$$

where $k_{\mathrm{C_3H_8}}$ is the reaction rate of $C_3H_8 + OH$. The value 0.736 is a result of the two channels of this reaction and is taken from Atkinson et al. (2006).

Besides emissions, Eq. (12) is another important source for atmospheric acetone (e.g., Jacob et al., 2002).

Geosci. Model Dev. Discuss., doi:10.5194/gmd-2016-259, 2016
Manuscript under review for journal Geosci. Model Dev.
Published: 24 October 2016

Geoscientific Model Development Discussions

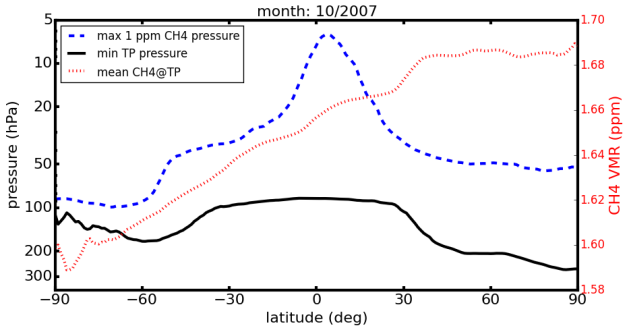

Figure 7. Zonal minimum of tropopause pressure, zonal maximum of 1 ppmv CH_4 pressure and zonal mean of CH_4 VMR at tropopause (right y-axis) for October 2007 of the OH-chem simulation (see Sect. 6). The 1 ppmv CH_4 pressure in each column is calculated as the air pressure of the model layer where CH_4 VMR decreases below 1 ppmv.

4.2 Above the UTLS region

The reaction system, described in Sect. 4.1, is valid in the troposphere, only (Jacob, 1999).

In the stratosphere, the lower VMRs of CO and CH_4 in Eq. (6) lead to increases of OH up to 10^8 molec cm^{-3} in the highest model layer (about 2 Pa). According to Brasseur and Solomon (1995), however, the OH number concentration in this altitude is in the order of 10^6 molec cm^{-3}. This overestimation of the OH concentration in ICON-ART results in too short lifetimes of the tracers and that is why the lifetime of the species is parametrised in another way for stratospheric conditions.

However, the loss rate of acetone with Eq. (10) is also realistic above the UTLS region due to the photolytic reactions (R10) and (R11).

Therefore, another mechanism is applied above the UTLS region (indicated by the dashed blue line in Fig. 7) only if no other term is added to the loss rate. The lifetime of CH_4 is parametrised pressure-dependent like in the Integrated Forecast System (IFS)[1]. In this parametrisation, the CH_4 lifetime in the troposphere is effectively infinite and decreases for pressure below 100 hPa, e.g. it is 2000 days at a pressure of 10 hPa. The CO lifetime is parametrised in the same way as in the KASIMA model (Karlsruhe SImulation model of the Middle Atmosphere) which also depends on pressure, only (Ruhnke et al., 1999; Kouker et al., 1999). The CO lifetime in this parametrisation in an altitude of 100 hPa is about 1 year and in 10 hPa it is 25 days. The formulae of these two lifetime parametrisations have been published by Stassen (2015). The lifetime of propane is set globally to 14 days (Rosado-Reyes and Francisco, 2007).

In order to be able to investigate processes within the UTLS region, a threshold in CH_4 of 1 ppmv ($= 10^{-6}$ mol mol^{-1}) is applied to decide whether OH mechanism or stratospheric parametrisation is used for the lifetime of the compounds, see Fig. 7. In this figure, the zonal maximum of the air pressure where CH_4 VMR decreases below 1 ppmv is illustrated along with the zonal minimum of the WMO tropopause pressure (see Sect. 2.1). The air pressure corresponding to 1 ppmv CH_4 is lower than the tropopause height on the whole latitude range with a minimum difference of about 50 hPa which means that

[1] http://www.ecmwf.int/sites/default/files/IFS_CY40R1_Part4.pdf

Geosci. Model Dev. Discuss., doi:10.5194/gmd-2016-259, 2016
Manuscript under review for journal Geosci. Model Dev.
Published: 24 October 2016

Table 5. Technical description of the simulations used in this study. For the used emission inventories see Table 3. Horizontal resolution for the simulations is R2B04 with model time step of 460 s. Output is given on model layers.

simulation name	time range	output interval (in h)	short description
constL(off)	2004-2015	23	constant lifetime, offline emissions
constL(onl)	2004-2015	23	constant lifetime, biogenic online emissions
OH-chem(off)	2004-2015	23	tracer depletion with OH, offline emissions
OH-chem(onl)	2004-2015	23	tracer depletion with OH, biogenic online emissions

the UTLS region can be investigated using the threshold of $1\,\mathrm{ppmv}$ in the CH_4 VMR. Figure 7 also includes the CH_4 VMR at the tropopause height. As the mainly anthropogenic CH_4 emission sources are mostly present in the northern hemisphere, the CH_4 VMR is higher in the northern than in the southern hemisphere.

5 The IAGOS-CARIBIC project

In this study, we aim to compare our simulations of acetone with airborne measurements in the UTLS region in a similar way as recently published by Jöckel et al. (2016).

In the ongoing project Civil Aircraft for the Regular Investigation of the atmosphere Based on an Instrument Container (IAGOS-CARIBIC) a fully automated laboratory has been integrated into a modified cargo container (Brenninkmeijer et al., 2007). Measuring about 100 trace gases and aerosol parameters, the IAGOS-CARIBIC laboratory is regularly placed on-board a Lufthansa Airbus 340-600 passenger aircraft for up to six consecutive flights per month. The cruising altitude of the aircraft coincides with the UTLS region where measurements have been rare previously. Between 2005 and 2014, the flights took off in Frankfurt whereas the flights nowadays start in Munich in Germany to many intercontinental destinations.

We use the acetone measurements from IAGOS-CARIBIC to compare them with the different innovations in ICON-ART (see Sect. 7). For our calculations, we use the data of flights 110 to 261 and 373 to 528.

6 Description of the ICON-ART simulations

We selected four simulations which are called constL(off), constL(onl), OH-chem(off) and OH-chem(onl). They are also summarised in Table 5 from a technical point of view.

The simulations are performed with a horizontal resolution of R2B04 (characteristic length of about $160\,\mathrm{km}$). For output, they are interpolated to a regular 1°x1° longitude-latitude grid. The lowest 46 of total 90 vertical layers are illustrated in Fig. 1. The model time step is set to $460\,\mathrm{s}$. All the simulations include an output interval of 23 hours because of the tracers' lifetime in the order of several days to months and therefore a negligible diurnal cycle in the tracer concentrations. Nevertheless, we can

Geosci. Model Dev. Discuss., doi:10.5194/gmd-2016-259, 2016
Manuscript under review for journal Geosci. Model Dev.
Published: 24 October 2016

consider the temporal variability of OH with this output interval. Emissions as described in Table 3 are added to the tracers' VMR in the lowest model layer.

The meteorological variables such as temperature, pressure and three-dimensional wind as well as sea surface temperature and sea ice cover are initialised with ERA-Interim on 1 January 2004 at 00 UTC in order to cover the IAGOS-CARIBIC time range (2005 – 2015) with a spin-up period of one year for the chemical tracers. CO and CH_4 are initialised based on mean values provided by Monitoring atmospheric composition and climate (MACC) reanalyses of January 2004 (Inness et al., 2013). C_3H_8 is initialised based on Pozzer et al. (2010). The initial volume mixing ratio of acetone is set globally to $1\,\mathrm{pptv}$. After initialisation ICON-ART runs freely.

constL(off): The simulation using constant lifetime is the reference simulation for the other simulations. In this simulation, acetone lifetime is set globally to $28\,\mathrm{days}$. This is the mean value of the chemical lifetimes of Jacob et al. (2002), Arnold et al. (2005), Fischer et al. (2012) and Khan et al. (2015). The lifetime of C_3H_8 is set to $14\,\mathrm{days}$. That of CO and CH_4 are parametrised as described in Sect. 4.2.

constL(onl): Simulation of online biogenic emissions of acetone is performed in this simulation where the offline biogenic acetone emissions in constL(off) are replaced by MEGAN-Online LAI.

OH-chem(off): In the simulation including the simplified OH chemistry, the mechanism as illustrated in Sect. 4 is used for depletion of the tracers and therefore replaces the constant lifetime of constL(off).

OH-chem(onl): In this simulation, the biogenic emissions of acetone are replaced by MEGAN-Online LAI. Apart from that, the configuration is the same as for OH-chem(off).

7 Results

In Figure 8, profiles of the annual mean acetone global lifetime according to Eq. (11) during the OH-chem(off) simulation are shown. For pressures higher than $900\,\mathrm{hPa}$, the photolysis rates in Eq. (10) get lower which means that the lifetime is dominated by the depletion with OH, only, leading to lifetimes up to $70\,\mathrm{days}$. In the troposphere and UTLS region, both mechanisms seem to have significant influence on the acetone lifetime. Due to the decrease in water vapour above the tropopause the production of OH by Reaction (R4) decreases. Additionally, the photolysis rates increase in the stratosphere for pressures below $50\,\mathrm{hPa}$ so that the influence of the OH depletion is negligible and the acetone lifetime decreases below one day.

When calculating the mean tropospheric lifetime of acetone according to Eq. (11) in the OH-chem simulations, we derive a value (33 days) comparable to the one (35 days) by Arnold et al. (2005) who also used the definition of SPARC to calculate the acetone lifetime.

Due to the seasonal variability in the biogenic emissions of acetone, its VMR in the mid-latitude UTLS region shows an annual variability with maximum values above $1500\,\mathrm{pptv}$ during summer (Sprung and Zahn, 2010; Elias et al., 2011; Neumaier et al., 2014). This is shown in Fig. 9 where the acetone seasonal cycle $\pm 3\,\mathrm{km}$ around the tropopause is derived from the IAGOS-CARIBIC measurements (panel a) and from the ICON-ART simulations described in Sect. 6.

Geosci. Model Dev. Discuss., doi:10.5194/gmd-2016-259, 2016
Manuscript under review for journal Geosci. Model Dev.
Published: 24 October 2016

Geoscientific Model Development Discussions

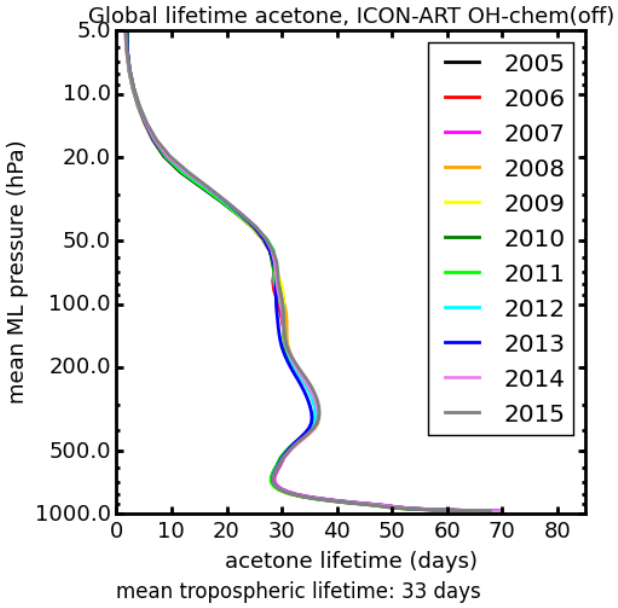

Figure 8. Global lifetime of acetone according to Eq. (11) in the OH-chem simulations averaged for each year. Definition of global lifetime by SPARC (2013) evaluated at each model layer.

In the panels of Fig. 9, the simulated acetone VMR is linearly interpolated in pressure, longitude, latitude and time to the IAGOS-CARIBIC flights (see Eckstein et al., 2016). For calculation of the tropopause height we use the data sets which are most convenient for the measurements and simulations: the underlying temperature profiles for tropopause height in the IAGOS-CARIBIC measurements are derived from ERA-Interim profiles whereas the simulated tropopause height is calculated directly during operation of ICON-ART (see Sect. 2.1). We limit the IAGOS-CARIBIC flights (and correspondingly the model data) to latitudes between 35 and 75° N and exclude descents and ascents of the aeroplane by using data inside the pressure range of 280 and 180 hPa (similar to Jöckel et al., 2016).

Figure 9 demonstrates that the general annual cycle of acetone can be reproduced with ICON-ART. Maximal values in the acetone VMR of all ICON-ART simulations occur between June and August where also the measurements maximise. However, differences in the magnitude can be seen: For the simulations driven by offline emissions (middle column) the maximum acetone VMR is underestimated by a factor of 3 with respect to the measurements.

Several reasons could explain this underestimation: (1) The constant acetone lifetime of 28 days is too low by a factor of at least 2. This is most unlikely as this value is the mean value of literature values (see Sect. 6) and Fig. 8 suggests a chemical lifetime of acetone in this order of magnitude using the simplified OH chemistry. (2) We account for chemical production of acetone due to reaction of propane with OH but neglect the contribution of other VOCs such as monoterpenes so that the acetone VMR could be too low. On the other hand, we neglect the uptake of acetone by the oceans and dry deposition which would decrease the acetone VMR (Fischer et al., 2012; Khan et al., 2015). (3) The emissions of acetone might be too low.

Geosci. Model Dev. Discuss., doi:10.5194/gmd-2016-259, 2016
Manuscript under review for journal Geosci. Model Dev.
Published: 24 October 2016

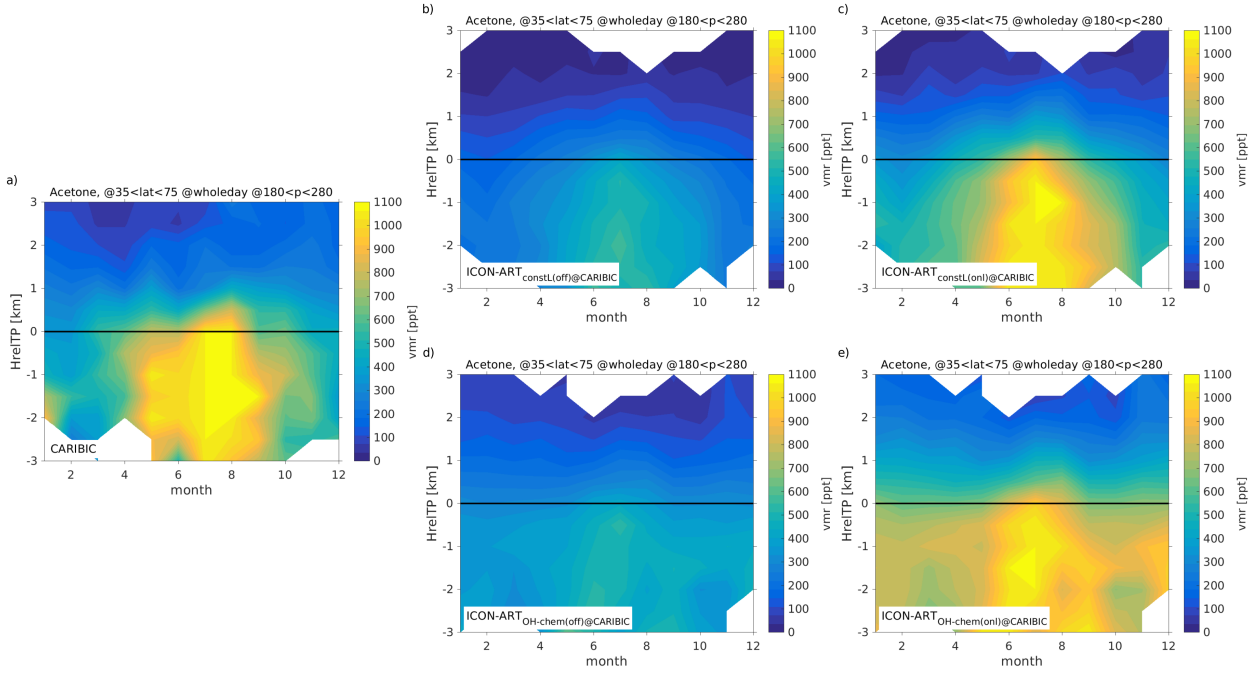

Figure 9. Annual cycles of the acetone VMR of (a) IAGOS-CARIBIC measurements and due to offline MEGAN-MACC (middle column) and MEGAN-Online biogenic emissions (right column) $\pm 3\,\mathrm{km}$ around the WMO tropopause for constL (first row) and OH-chem simulations (second row). The acetone VMR in the IAGOS-CARIBIC measurements increases up to $1700\,\mathrm{pptv}$ in the maximum.

Emission data sets generally are highly uncertain. Sindelarova et al. (2014) estimated an uncertainty in the isoprene emissions of $14\,\%$ for the MEGAN-MACC data set. For other VOCs, it could be even higher (e.g. $48.5\,\%$ by Williams et al., 2013).

Due to the latter reason, we choose the larger online emission with the original leaf area index of ICON (red line in Fig. 6) for our comparison to the measurements. As these emissions are more than twice larger than the offline emissions the acetone VMR is increased in the UTLS region correspondingly. Thus, the differences with reference to observations are reduced but the highest values in the measurements can still not be reached (around $1100\,\mathrm{pptv}$ compared to $1700\,\mathrm{pptv}$ in the measurements). Apart from the values in the maximum, Fig. 9c using MEGAN-Online LAI combined with constant lifetime of acetone shows the best agreement with the observations in the upper troposphere: the acetone VMR during winter and "near-summer" only differs by $100\,\mathrm{pptv}$ or below.

As already mentioned above, the global lifetime of acetone in the OH-chem simulations with a value of $33\,\mathrm{days}$ is in the same order of magnitude as in the constL simulations. That is why the maximum values in the acetone VMR in the OH-chem simulations are comparable to the corresponding constL simulations. However, differences occur during winter where the clearly higher acetone lifetime of about $1.5\,\mathrm{years}$ in the OH-chem simulations increases the acetone VMR in the UTLS region.

Geosci. Model Dev. Discuss., doi:10.5194/gmd-2016-259, 2016
Manuscript under review for journal Geosci. Model Dev.
Published: 24 October 2016

The comparison of Fig. 9e with the observations demonstrates that the acetone VMR is overestimated by a factor of about 1.5 in the winter months December to February in the upper troposphere. In the lowermost stratosphere and especially above 2 km of the tropopause height, though, the acetone VMR is improved using the OH chemistry where the observations show higher VMRs than for the case of a constant lifetime (Fig. 9c).

8 Conclusions

We introduce the new interface for including emissions from external data sources in ICON-ART. The interface reads the data interpolated to the ICON grid, interpolates it to the simulation time and adds it to the trace gas volume mixing ratio in ICON-ART. In addition, we demonstrate the online biogenic emission model MEGAN2.1 in the configuration as implemented in ICON-ART. Furthermore, we present a simplified parametrisation to deplete chemical species by reaction with OH. The OH concentration is calculated as steady state: it is produced by photolysis of ozone and reaction of the produced $O(^1D)$ with water vapour. It is depleted by reactions with CH_4 and CO.

With these new features, it is now possible to simulate volatile compounds (VOCs) with ICON-ART reliably. We illustrate this with acetone as one member of the VOCs.

We investigate the influence of the different features by comparing them to airborne measurements of the IAGOS-CARIBIC project in the upper troposphere and lowermost stratosphere (UTLS). We test two parametrisations of the leaf area index (LAI) in MEGAN2.1 for October 2007: emissions using the LAI of ICON are twice as high than the emissions of the offline emission inventory MEGAN-MACC. The emissions due to the parametrised LAI according to Dai et al. (2004) are comparable to MEGAN-MACC in terms of global means and can therefore be used for investigating the influence of the diurnal cycle on acetone in the atmosphere. In order to account for the uncertainty in the emission inventories we show results of MEGAN2.1 using the LAI of ICON.

With offline emissions the acetone VMR in the UTLS region is underestimated by factor of 3. Correspondingly, it is increased by replacing offline with online biogenic emissions. The simplified OH chemistry leads to a higher acetone lifetime especially during winter which results in an overestimation of the acetone VMR within December and February by a factor of about 1.5. On the other hand, the acetone VMR in the lowermost stratosphere is improved by using the OH depletion mechanism.

Altogether, we show that the general acetone annual cycle is well represented in the model compared to the airborne IAGOS-CARIBIC measurements with a maximum during summer and a minimum during winter. Considering the acetone distribution in the lowest model layer we demonstrate that the presented emission interface performs well. In addition, the calculated tropospheric acetone lifetime of 33 days is in good agreement with Arnold et al. (2005) who used the same method to derive it. This value suggests that the new parametrisation of tracer depletion with OH is a good estimate of the OH concentration in the troposphere.

Geosci. Model Dev. Discuss., doi:10.5194/gmd-2016-259, 2016
Manuscript under review for journal Geosci. Model Dev.
Published: 24 October 2016

Geoscientific Model Development Discussions
Open Access
EGU

Code availability

Currently the legal departments of MPI and DWD are finalising the ICON license. If you want to obtain ICON-ART you will first need to sign an ICON license which you will get at http://www.mpimet.mpg.de/en/science/models/model-distribution.html. In a second step you will get the ART code after signing the ICON-ART license which will be available at http://ICON-ART.imk-tro.kit.edu/.

Appendix A: Predictor-corrector method

Concentrations of tracers are determined by solving the following differential equation:

$$\frac{\mathrm{d}c_i}{\mathrm{d}t} = P_i - c_i\, L_i \tag{A1}$$

with c_i, P_i and L_i as concentration, chemical production and loss rate of tracer i. In ICON-ART version 1.0, this equation was discretised with the explicit Euler method, omitting the index i (Rieger et al., 2015):

$$c_{n+1} = c_n + (P_n - c_n\, L_n) \cdot \Delta t \tag{A2}$$

In this equation, the index n stands for the nth model time step. Too low values of the tracer's lifetime can lead to solutions that do not converge to the differential equation (A1). Since fully implicit methods generally are expensive in computation resources, Seinfeld and Pandis (2012) suggest a two-step predictor-corrector discretisation method for solving Eq. (A1) which is discussed in this section. This method reasonably closes the gap between the low computation effort for explicit discretisation methods on the one hand and the accuracy and stability of implicit methods on the other hand.

Please note that the lifetime in this section is the reciprocal value of the loss rate (compared to the definition of SPARC used in the other sections).

Generally, Equation (A1) can be discretised implicitly as follows (Seinfeld and Pandis, 2012):

$$c_{n+1} = \frac{c_n \cdot (\tau_{n+1} + \tau_n - \Delta t) + 0.5\,\Delta t\,(P_{n+1} + P_n)\,(\tau_{n+1} + \tau_n)}{\tau_{n+1} + \tau_n + \Delta t} \tag{A3}$$

Lifetimes and productions of the next time step, denoted by index $n+1$, are not defined at time step n. That is why they have to be approximated before Eq. (A3) can be evaluated.

In a first step, called the predictor step, the new concentrations c_* are approximated by assuming constant lifetime and production ($\tau_{n+1} = \tau_n$ and $P_{n+1} = P_n$):

$$c_* = \frac{c_n \cdot (2\,\tau_n - \Delta t) + 2\Delta t\,\tau_n\,P_n}{2\,\tau_n + \Delta t} \tag{A4}$$

Geosci. Model Dev. Discuss., doi:10.5194/gmd-2016-259, 2016
Manuscript under review for journal Geosci. Model Dev.
Published: 24 October 2016

Geoscientific Model Development Discussions
Open Access
EGU

In this study, these concentrations are calculated for CH_4, CO, propane and acetone. This is an inaccurate estimation of the concentrations of the next time step since lifetime and production both can vary within one time step (Seinfeld and Pandis, 2012). For improving accuracy, the lifetimes and productions of the next time step are approximated with the c_* of Eq. (A4). For that purpose, c_* is used for calculating a new OH number concentration, $[\mathrm{OH}]_*$, as described in Sect. 4.1. In turn, with $[\mathrm{OH}]_*$, the lifetimes and chemical productions of the next time step can be approximated, denoted as τ_* and P_*, respectively.

Then, the so-called corrector step can be executed in order to get the tracer concentrations of the next time step by replacing τ_{n+1} and P_{n+1} in Eq. (A3) by their approximations τ_* and P_*, respectively:

$$c_{n+1} = \frac{c_n \cdot (\tau_* + \tau_n - \Delta t) + 0.5\,\Delta t\,(P_* + P_n)\,(\tau_* + \tau_n)}{\tau_* + \tau_n + \Delta t} \tag{A5}$$

If the expression $\tau_* + \tau_n$ gets lower than Δt, this method also gets instable. That is why we use the fully implicit method assuming constant lifetime and chemical production if the lifetime gets lower than Δt:

$$c_{n+1} = P_n\,\tau_n + (c_n - P_n\,\tau_n) \cdot \exp\left(-\frac{\Delta t}{\tau_n}\right), \quad \tau_n < \Delta t \tag{A6}$$

Acknowledgements. We acknowledge ECCAD for archiving and distributing the data. This study was performed on the computational resource ForHLR II funded by the Ministry of Science, Research and the Arts Baden-Württemberg and DFG ("Deutsche Forschungsgemeinschaft").

Geosci. Model Dev. Discuss., doi:10.5194/gmd-2016-259, 2016
Manuscript under review for journal Geosci. Model Dev.
Published: 24 October 2016

References

Arnold, S., Chipperfield, M., and Blitz, M.: A three-dimensional model study of the effect of new temperature-dependent quantum yields for acetone photolysis, J. Geophys. Res.: Atmosphere, 110, doi:10.1029/2005JD005998, 2005.

Atkinson, R. and Arey, J.: Atmospheric Degradation of Volatile Organic Compounds, Chemical Reviews, 103, 4605–4638, doi:10.1021/cr0206420, 2003.

Atkinson, R., Baulch, D. L., Cox, R. A., Crowley, J. N., Hampson, R. F., Hynes, R. G., Jenkin, M. E., Rossi, M. J., Troe, J., and Subcommittee, I.: Evaluated kinetic and photochemical data for atmospheric chemistry: Volume II - gas phase reactions of organic species, Atmos. Chem. Phys., 6, 3625–4055, doi:10.5194/acp-6-3625-2006, 2006.

Blake, N. and Blake, D.: Tropospheric Chemistry and Composition: VOCs: Overview in Encyclopedia of Atmospheric Sciences Edited by J. R. Holton, J. A. Pyle, and J. A. Curry, Academic Press, doi:10.1006/rwas.2002.0422, 2002.

Boucher, O., Haigh, J., Hauglustaine, D., Haywood, J., Myhre, G., Nakajima, T., Shi, G., and Solomon, S., eds.: *Radiative Forcing of Climate Change. In:* Climate Change 2001: The Scientific Basis. Contribution of Working Group I to the Third Assessment Report of the Intergovernmental Panel on Climate Change, Cambridge University Press, Cambridge, United Kingdom and New York, NY, USA, 2001.

Brasseur, G. and Solomon, S.: Aeronomy of the Middle Atmosphere, Atmospheric sciences library, D. Reidel Publishing Company, Dordrecht, 2nd edn., 1995.

Brenninkmeijer, C., Crutzen, P., Boumard, F., Dauer, T., Dix, B., Ebinghaus, R., Filippi, D., Fischer, H., Franke, H., Frieß, U., et al.: Civil Aircraft for the regular investigation of the atmosphere based on an instrumented container: The new CARIBIC system, Atmos. Chem. Phys., 7, 4953–4976, doi:10.5194/acp-7-4953-2007, 2007.

Dai, Y., Dickinson, R., and Wang, Y.: A Two-Big-Leaf Model for Canopy Temperature, Photosynthesis, and Stomatal Conductance, J. Climate, 17, 2281–2299, doi:10.1175/1520-0442(2004)017<2281:ATMFCT>2.0.CO;2, 2004.

Diehl, T., Heil, A., Chin, M., Pan, X., Streets, D., Schultz, M., and Kinne, S.: Anthropogenic, biomass burning, and volcanic emissions of black carbon, organic carbon, and SO_2 from 1980 to 2010 for hindcast model experiments, Atmos. Chem. Phys. Discuss., 12, 24 895–24 954, doi:10.5194/acpd-12-24895-2012, 2012.

Doms, G. and Schättler, U.: A description of the nonhydrostatic regional model LM. Part II: Physical parameterization, Tech. rep., Deutscher Wetterdienst, Offenbach, 2004.

Dunlea, E. J. and Ravishankara, A. R.: Measurement of the rate coefficient for the reaction of $O(^1D)$ with H_2O and re-evaluation of the atmospheric OH production rate, Phys. Chem. Chem. Phys., 6, 3333–3340, doi:10.1039/B402483D, 2004.

Eckstein, J., Ruhnke, R., Zahn, A., Neumaier, M., Kirner, O., and Braesicke, P.: An assessment of the climatological representativeness of IAGOS-CARIBIC trace gas measurements using EMAC model simulations, Atmos. Chem. Phys. Discuss., 2016, 1–25, doi:10.5194/acp-2016-179, 2016.

Elias, T., Szopa, S., Zahn, A., Schuck, T., Brenninkmeijer, C., Sprung, D., and Slemr, F.: Acetone variability in the upper troposphere: analysis of CARIBIC observations and LMDz-INCA chemistry-climate model simulations, Atmos. Chem. Phys., 11, 8053–8074, doi:10.5194/acp-11-8053-2011, 2011.

Elshorbany, Y. F., Duncan, B. N., Strode, S. A., Wang, J. S., and Kouatchou, J.: The description and validation of the computationally Efficient CH4-CO-OH (ECCOHv1.01) chemistry module for 3-D model applications, Geosci. Model Dev., 9, 799–822, doi:10.5194/gmd-9-799-2016, 2016.

Geosci. Model Dev. Discuss., doi:10.5194/gmd-2016-259, 2016
Manuscript under review for journal Geosci. Model Dev.
Published: 24 October 2016

Field, C. B., Randerson, J. T., and Malmström, C. M.: Global net primary production: Combining ecology and remote sensing, Remote Sens. Environ., 51, 74 – 88, doi:10.1016/0034-4257(94)00066-V, 1995.

Fischer, E., Jacob, D. J., Millet, D., Yantosca, R. M., and Mao, J.: The role of the ocean in the global atmospheric budget of acetone, Geophys. Res. Lett., 39, doi:10.1029/2011GL050086, L01807, 2012.

Folkins, I. and Chatfield, R.: Impact of acetone on ozone production and OH in the upper troposphere at high NO_x, J. Geophys. Res.: Atmospheres, 105, 11 585–11 599, doi:10.1029/2000JD900067, 2000.

Granier, C., Bessagnet, B., Bond, T., D'Angiola, A., Denier van der Gon, H., Frost, G., Heil, A., Kaiser, J., Kinne, S., Klimont, Z., Kloster, S., Lamarque, J.-F., Liousse, C., Masui, T., Meleux, F., Mieville, A., Ohara, T., Raut, J.-C., Riahi, K., Schultz, M., Smith, S., Thompson, A., van Aardenne, J., van der Werf, G., and van Vuuren, D.: Evolution of anthropogenic and biomass burning emissions of air pollutants at global and regional scales during the 1980-2010 period, Climatic Change, 109, 163–190, doi:10.1007/s10584-011-0154-1, 2011.

Guenther, A., Jiang, X., Heald, C., Sakulyanontvittaya, T., Duhl, T., Emmons, L., and Wang, X.: The Model of Emissions of Gases and Aerosols from Nature version 2.1 (MEGAN2.1): an extended and updated framework for modeling biogenic emissions, Geosci. Model Dev., 5, 1471–1492, doi:10.5194/gmd-5-1471-2012, 2012.

Heikes, B. G., Chang, W., Pilson, M. E. Q., Swift, E., Singh, H. B., Guenther, A., Jacob, D. J., Field, B. D., Fall, R., Riemer, D., and Brand, L.: Atmospheric methanol budget and ocean implication, Global Biogeochem. Cycles, 16, 80–1–80–13, doi:10.1029/2002GB001895, 1133, 2002.

Hollingsworth, A., Engelen, R., Benedetti, A., Dethof, A., Flemming, J., Kaiser, J., Morcrette, J., Simmons, J., Textor, C., Boucher, O., Chevallier, F., Rayner, P., Elbern, H., Eskes, H., Granier, C., Peuch, V., Rouil, L., and Schultz, M.: Toward a monitoring and forecasting system for atmospheric composition: the GEMS project, Bull. Amer. Meteor. Soc., 89, 1147–1164, doi:10.1175/2008BAMS2355.1, 2008.

Inness, A., Baier, F., Benedetti, A., Bouarar, I., Chabrillat, S., Clark, H., Clerbaux, C., Coheur, P., Engelen, R. J., Errera, Q., Flemming, J., George, M., Granier, C., Hadji-Lazaro, J., Huijnen, V., Hurtmans, D., Jones, L., Kaiser, J. W., Kapsomenakis, J., Lefever, K., Leitão, J., Razinger, M., Richter, A., Schultz, M. G., Simmons, A. J., Suttie, M., Stein, O., Thépaut, J.-N., Thouret, V., Vrekoussis, M., Zerefos, C., and the MACC team: The MACC reanalysis: an 8 yr data set of atmospheric composition, Atmos. Chem. Phys., 13, 4073–4109, doi:10.5194/acp-13-4073-2013, 2013.

Jacob, D. J.: Introduction to atmospheric chemistry, Princeton Univ. Press, Princeton, NJ, 1st edn., 1999.

Jacob, D. J., Field, B. D., Jin, E. M., Bey, I., Li, Q., Logan, J. A., Yantosca, R. M., and Singh, H. B.: Atmospheric budget of acetone, J. Geophys. Res.: Atmosphere, 107, ACH 5–1–ACH 5–17, doi:10.1029/2001JD000694, 2002.

Jaeglé, L., Jacob, D. J., Brune, W., Tan, D., Faloona, I., Weinheimer, A., Ridley, B., Campos, T., and Sachse, G.: Sources of HOx and production of ozone in the upper troposphere over the United States, Geophys. Res. Lett., 25, 1709–1712, doi:10.1029/98GL00041, 1998.

Janssens-Maenhout, G., Petrescu, A. M., Muntean, M., and Blujdea, V.: Verifying Greenhouse Gas Emissions: Methods to Support International Climate Agreements, Greenhouse Gas Measurement and Management, 1, 132–133, doi:10.1080/20430779.2011.579358, 2011.

Janssens-Maenhout, G., Diego, V., and Marilena Muntean, G.: Global emission inventories in the Emission Database for Global Atmospheric Research (EDGAR)–Manual (I), Gridding: EDGAR emissions distribution on global gridmaps, Publications Office of the European Union, Luxembourg, 2013.

Jöckel, P., Tost, H., Pozzer, A., Kunze, M., Kirner, O., Brenninkmeijer, C. A. M., Brinkop, S., Cai, D. S., Dyroff, C., Eckstein, J., Frank, F., Garny, H., Gottschaldt, K.-D., Graf, P., Grewe, V., Kerkweg, A., Kern, B., Matthes, S., Mertens, M., Meul, S., Neumaier, M., Nützel, M., Oberländer-Hayn, S., Ruhnke, R., Runde, T., Sander, R., Scharffe, D., and Zahn, A.: Earth System Chemistry integrated Modelling

(ESCiMo) with the Modular Earth Submodel System (MESSy) version 2.51, Geosci. Model Dev., 9, 1153–1200, doi:10.5194/gmd-9-1153-2016, 2016.

Keller, C. A., Long, M. S., Yantosca, R. M., Da Silva, A. M., Pawson, S., and Jacob, D. J.: HEMCO v1.0: a versatile, ESMF-compliant component for calculating emissions in atmospheric models, Geosci. Model Dev., 7, 1409–1417, doi:10.5194/gmd-7-1409-2014, 2014.

Kerkweg, A., Sander, R., Tost, H., and Jöckel, P.: Technical note: Implementation of prescribed (OFFLEM), calculated (ONLEM), and pseudo-emissions (TNUDGE) of chemical species in the Modular Earth Submodel System (MESSy), Atmos. Chem. Phys., 6, 3603–3609, doi:10.5194/acp-6-3603-2006, 2006.

Khan, M., Cooke, M., Utembe, S., Archibald, A., Maxwell, P., Morris, W., Xiao, P., Derwent, R., Jenkin, M., Percival, C., Walsh, R., Young, T., Simmonds, P., Nickless, G., O'Doherty, S., and Shallcross, D.: A study of global atmospheric budget and distribution of acetone using global atmospheric model STOCHEM-CRI, Atmos. Environ., 112, 269 – 277, doi:10.1016/j.atmosenv.2015.04.056, 2015.

Kouker, W., Offermann, D., Küll, V., Reddmann, T., Ruhnke, R., and Franzen, A.: Streamers observed by the CRISTA experiment and simulated in the KASIMA model, J. Geophys. Res.: Atmospheres, 104, 16 405–16 418, doi:10.1029/1999JD900177, 1999.

Lamarque, J.-F., Bond, T. C., Eyring, V., Granier, C., Heil, A., Klimont, Z., Lee, D., Liousse, C., Mieville, A., Owen, B., Schultz, M. G., Shindell, D., Smith, S. J., Stehfest, E., Van Aardenne, J., Cooper, O. R., Kainuma, M., Mahowald, N., McConnell, J. R., Naik, V., Riahi, K., and van Vuuren, D. P.: Historical (1850-2000) gridded anthropogenic and biomass burning emissions of reactive gases and aerosols: methodology and application, Atmos. Chem. Phys., 10, 7017–7039, doi:10.5194/acp-10-7017-2010, 2010.

Lauritzen, P. H., Erath, C., and Mittal, R.: On simplifying 'incremental remap' - based transport schemes, J. Comp. Phys., 230, 7957 – 7963, doi:10.1016/j.jcp.2011.06.030, 2011.

Leuenberger, D., Koller, M., Fuhrer, O., and Schär, C.: A generalization of the SLEVE vertical coordinate, Mon. Wea. Rev., 138, 3683–3689, doi:10.1175/2010MWR3307.1, 2010.

Miura, H.: An Upwind-Biased Conservative Advection Scheme for Spherical Hexagonal-Pentagonal Grids, Mon. Wea. Rev., 135, 4038–4044, doi:10.1175/2007MWR2101.1, 2007.

Neumaier, M., Ruhnke, R., Kirner, O., Ziereis, H., Stratmann, G., Brenninkmeijer, C., and Zahn, A.: Impact of acetone (photo) oxidation on HOx production in the UT/LMS based on CARIBIC passenger aircraft observations and EMAC simulations, Geophys. Res. Lett., 41, 3289–3297, doi:10.1002/2014GL059480, 2014.

Potter, C. S., Randerson, J. T., Field, C. B., Matson, P. A., Vitousek, P. M., Mooney, H. A., and Klooster, S. A.: Terrestrial ecosystem production: a process model based on global satellite and surface data, Glob. Biogeochem. Cy., 7, 811–841, 1993.

Pozzer, A., Pollmann, J., Taraborrelli, D., Jöckel, P., Helmig, D., Tans, P., Hueber, J., and Lelieveld, J.: Observed and simulated global distribution and budget of atmospheric C₂-C₅ alkanes, Atmos. Chem. Phys., 10, 4403–4422, doi:10.5194/acp-10-4403-2010, 2010.

Prather, M. J.: Photolysis rates in correlated overlapping cloud fields: Cloud-J 7.3c, Geosci. Model Dev., 8, 2587–2595, doi:10.5194/gmd-8-2587-2015, 2015.

Prill, F.: DWD ICON Tools Documentation (software revision 764), Deutscher Wetterdienst, Offenbach, 2016.

Randerson, J. T., Thompson, M. V., Malmström, C. M., Field, C. B., and Fung, I. Y.: Substrate limitations for heterotrophs: Implications for models that estimate the seasonal cycle of atmospheric CO_2, Glob. Biogeochem. Cy., 10, 585–602, doi:10.1029/96GB01981, 1996.

Rieger, D., Bangert, M., Bischoff-Gauss, I., Förstner, J., Lundgren, K., Reinert, D., Schröter, J., Vogel, H., Zängl, G., Ruhnke, R., and Vogel, B.: ICON-ART 1.0 - a new online-coupled model system from the global to regional scale, Geosci. Model Dev., 8, 1659–1676, doi:10.5194/gmd-8-1659-2015, 2015.

Rosado-Reyes, C. M. and Francisco, J. S.: Atmospheric oxidation pathways of propane and its by-products: Acetone, acetaldehyde, and propionaldehyde, J. Geophys. Res.: Atmosphere, 112, doi:10.1029/2006JD007566, D14310, 2007.

Ruhnke, R., Kouker, W., and Reddmann, T.: The influence of the $OH + NO_2 + M$ reaction on the NO_y, partitioning in the late Arctic winter 1992/1993 as studied with KASIMA, J. Geophys. Res.: Atmospheres, 104, 3755–3772, doi:10.1029/1998JD100062, 1999.

Sander, S., Abbatt, J., Barker, J., Burkholder, J., Friedl, R., Golden, D., Huie, R., Kolb, C., Kurylo, M., Moortgat, K., Orkin, V., and Wine, P.: Chemical Kinetics and Photochemical Data for Use in Atmospheric Studies, Evaluation No. 17, JPL Publication 10-6, 2011.

Seifert, A.: A short introduction to microphysics in the NWP ICON model, Tech. rep., Deutscher Wetterdienst, Offenbach, 2010.

Seinfeld, J. H. and Pandis, S. N.: Atmospheric Chemistry and Physics: From Air Pollution to Climate Change, John Wiley & Sons, 2nd edn., 2012.

Shao, M. and Wildt, J.: Quantification of acetone emission from pine plants, Sci. China, Ser. B Chem., 45, 532–540, doi:10.1360/02yb9070, 2002.

Sindelarova, K., Granier, C., Bouarar, I., Guenther, A., Tilmes, S., Stavrakou, T., Müller, J.-F., Kuhn, U., Stefani, P., and Knorr, W.: Global data set of biogenic VOC emissions calculated by the MEGAN model over the last 30 years, Atmos. Chem. Phys., 14, 9317–9341, doi:10.5194/acp-14-9317-2014, 2014.

Singh, H. B., Kanakidou, M., Crutzen, P., and Jacob, D.: High concentrations and photochemical fate of oxygenated hydrocarbons in the global troposphere, Nature, 378, 50–54, doi:10.1038/378050a0, 1995.

SPARC: SPARC Report on Lifetimes of Stratospheric Ozone-Depleting Substances, Their Replacements, and Related Species, Tech. rep., SPARC, 2013.

Sprung, D. and Zahn, A.: Acetone in the upper troposphere/lowermost stratosphere measured by the CARIBIC passenger aircraft: Distribution, seasonal cycle, and variability, J. Geophys. Res.: Atmosphere, 115, doi:10.1029/2009JD012099, 2010.

Stassen, C.: Simulation von chemischen Tracern mit ICON-ART, Master's thesis, Karlsruhe Institute of Technology (KIT), Germany, 2015.

van der Werf, G. R., Randerson, J. T., Giglio, L., Collatz, G. J., Kasibhatla, P. S., and Arellano Jr., A. F.: Interannual variability in global biomass burning emissions from 1997 to 2004, Atmos. Chem. Phys., 6, 3423–3441, doi:10.5194/acp-6-3423-2006, 2006.

van der Werf, G. R., Randerson, J. T., Giglio, L., Collatz, G. J., Mu, M., Kasibhatla, P. S., Morton, D. C., DeFries, R. S., Jin, Y., and van Leeuwen, T. T.: Global fire emissions and the contribution of deforestation, savanna, forest, agricultural, and peat fires (1997-2009), Atmos. Chem. Phys., 10, 11 707–11 735, doi:10.5194/acp-10-11707-2010, 2010.

Wan, H., Giorgetta, M. A., Zängl, G., Restelli, M., Majewski, D., Bonaventura, L., Fröhlich, K., Reinert, D., Rípodas, P., Kornblueh, L., and Förstner, J.: The ICON-1.2 hydrostatic atmospheric dynamical core on triangular grids - Part 1: Formulation and performance of the baseline version, Geosci. Model Dev., 6, 735–763, doi:10.5194/gmd-6-735-2013, 2013.

Williams, J., van Velthoven, P., and Brenninkmeijer, C.: Quantifying the uncertainty in simulating global tropospheric composition due to the variability in global emission estimates of Biogenic Volatile Organic Compounds, Atmos. Chem. Phys., 13, 2857–2891, doi:10.5194/acp-13-3693-2013, 2013.

World Meteorological Organization (WMO): Meteorology A Three-Dimensional Science: Second Session of the Commission for Aerology, WMO Bulletin IV, WMO, Geneva, 1957.

Zängl, G., Reinert, D., Rípodas, P., and Baldauf, M.: The ICON (ICOsahedral Non-hydrostatic) modelling framework of DWD and MPI-M: Description of the non-hydrostatic dynamical core, Quart. J. Roy. Meteor. Soc., 141, 563–579, doi:10.1002/qj.2378, 2015.